International Research Journal of Natural and Applied Sciences
ISSN: (2349-4077)
Impact Factor 7.032 Volume 10, Issue 12, December 2023
Website- www.aarf.asia, Email : editor@aarf.asia , editoraarf@gmail.com

# Multifaceted Characterization of Rare-Earth Doped BFO-BST ferovskites: A Study of Structural and Optical Properties

**Vinodkumar**
**(Research Scholar)**
**Dr. Priyanka Bansal(Associate Professor)**
**(Research Supervisor)**
**Glocal School Of Science**

**Abstract**
Due to their simultaneous ferroelectricity, ferromagnetism, and ferroelasticity, multiferroic nanomaterials have garnered attention for use in multifunctional, low-power, environmentally friendly devices. Bismuth ferrite (BiFeO3, BFO) is ferroelectric and (anti)ferromagnetic at ambient temperature. Structural and optical properties were explored for the predominant BFO-BST compound, [BiFeO3]0.5[(BaSr)0.5TiO3]. We then explored how rare-earth (RE) ion doping influenced the host compound's multiferroic properties. The crystal structures of the examined samples are revealed by integrating X-ray Diffraction patterns and Rietveld analysis. This paper describes rare-earth doped BFO BST perovskites' multiferroic and optical properties. This study explores rare-earth ions' structural and optical effects on BFO-BST.
***Keywords:****structural, diffraction, ions, crystal, consumption.*

## Introduction

Multiferroic and magnetoelectric (MF-ME) materials are extensively studied due to their distinctive features rooted in fundamental physics, which provide numerous potential applications in modern technology. Out of all the naturally occurring or chemically created MF-ME materials, BFO or BiFeO3, also known as Bismuth Ferrite, is the first material that has been identified as a ferro-magnetoelectric material. It has a rhombohedrally distorted perovskite crystal structure with the R3c or C63V symmetry at a temperature of TC=830oC and TN=400oC. Several inconsistencies in this system, including weak magnetic properties, small remnant polarization, high leakage, and low resistivity, limit its practical applications. To address this problem, extensive research is required to find suitable substitutions for various dopants at the necessary A and B sites. Materials that exhibit multiple ferroelectric, ferromagnetic, and ferro elastic characteristics in a single structure are known as multiferroic nanotechnology. The presence of many order characteristics in a single epitaxial phase is what has lately sparked a lot of interest in multiferroic semiconductors. As a result, it finds widespread use in eco-friendly, multi-purpose gadgets with low power consumption. At room temperature, the coupling of these features is desired for multiferroic nanoparticles.

## Materials and methods

### Sample Preparation Details

Our samples were made using 99.99% pure AR-grade oxides (Bi2O3, La2O3, Sm2O3, Nd2O3, Fe2O3, TiO2) and carbonates (BaCO3, SrCO3). A chemical balance is used to measure and obtain raw components based on stoichiometry. Each product's mixture was carefully mixed using an agate motor and pestle system for 3 hours in a dry state and 4 hours in a wet state with ethanol (a volatile solvent) to achieve a homogeneous mixture until it dried. Each clean alumina crucible was filled with the carefully dried fine powder combination and lidded. BFO-BST and Series-I samples (LA1, LA2,

LA3, LA4) were calcined at 900°C and 1000°C for 8 hours. Series-II (Nd1, Nd2, Nd3, Nd4) and Series-III (Sm1, Sm2, Sm3, Sm4) samples were calcined at 1100°C for 8 hours in a programmable high-temperature muffle furnace. Calcined furnace powders were lumps. These lumps were hand-ground fine. Sample phase purity and expected formation were examined using room temperature PXRD. Then, using an agate mortar and pestle, each sample's powder was mixed with 7% PVA binder. The powder was mixed with a binder and squeezed at low temperature to make cylindrical pellets. This was achieved by applying hydraulic pressure in a die-punch system at 5×108 kgm-2 iso-static pressure. BFO-BST pellets and Series-I samples were sintered at 150°C for 8 hours, whereas Series-II and III samples were sintered at 1150°C. This was done to create dense compounds. To conduct electrical measurements, all pellet surfaces were thoroughly polished using grit sandpaper. After coating the pellets with a high-quality silver paste, they were oven-dried for 2 hours at 150 degrees Celsius.

**Structural & Morphological Characterizations**

The samples were analyzed for their crystal structure and surface morphology using "Powder X-ray Diffraction (PXRD) and Scanning Electron Microscopy (SEM) techniques", respectively. The XRD data has been refined using Rietveld Analysis. The formation of compounds with the desired ratio of elements was verified using Energy Dispersive X-ray Analysis (EDAX).

**Results and discussion**

The crystal structure or phase formation of the produced samples was studied using "X-ray Diffraction measurements. The X-ray diffraction (XRD)" patterns of the BFO-BST and Series-II (Nd1 to Nd4) samples, respectively. The peak refinement process involved modifying various simulation conditions, such as background, scale factor, specimen displacement, zero shift, transparency, lattice parameters, full width half maxima (FWHM), shape parameters, atomic positions, preferred orientations, and anisotropic temperature parameters. Rietveld refinement validates the phase structure of the samples and provides the refined cell characteristics, presented in Table 1.

**Table 1. Structures, JCPDS, cell parameters and Reliability factors for BFO-BST & Series-II samples.**

| Samples | Structure | JCPDS No. / CODIDs | CellParameters(Å) | | | ReliabilityFactors | | | |
|---|---|---|---|---|---|---|---|---|---|
| | | | a | b | c | $R_{wp}$ (%) | $R_{exp}$ (%) | $R_b$ (%) | $\chi^2$ |
| BFO-BST | Distorted Orthorhombic (Pbnm) | 01-084-0106 | 5.607 | 5.607 | 12.743 | 8.24 | 7.44 | 5.64 | 1.16 |
| Nd1(x=0) | Tetragonal (P4mm) | 1522120 | 3.976 | 3.976 | 4.11 | 10.16 | 5.37 | 7.65 | 2.20 |
| Nd2(x=0.25) | | 1522121 | 3.964 | 3.964 | 3.972 | 12.29 | 6.54 | 6.15 | 1.70 |
| Nd3(x=0.5) | | 1522120 | 3.972 | 3.972 | 4.022 | 12.24 | 6.1 | 5.28 | 1.76 |
| Nd4(x=0.75) | | 1522122 | 3.962 | 3.962 | 3.966 | 10.62 | 5.75 | 5.31 | 1.61 |

The table also presents the reliability parameters of the completed refinement and the goodness of fit, which indicates that the refinement is deemed to be flawless. The measured values of the cell parameters (a, b, and c) are observed to grow when the ionic radii of the substituent on the A-site increase. Doping effects cause a deformation in the structure, which in turn affects the lattice parameters. The reflection peaks of all the samples have been matched with their corresponding (h k l) Miller indices. The crystallinity of the sample in the [BixNd(1-x)BaSr)0.5]0.5[FeTi]0.5O3 compound increases as the value of x ranges from 0 to 0.75. The observed phenomenon of peaks shifting towards lower 2θ values as the composition increases from x=0 to 0.75 may be attributed to the co-existence

of bismuth (Bi) and lanthanum (La) content, specifically the presence of heavier ions at the A-site. The Rietveld refined graphs of each sample are displayed in the inset of the corresponding XRD patterns, demonstrating a strong agreement between the experimental and computed data.

**Table 2. Tolerance factor, Crystallite size & Strain of BFO-BST & Series-II samples.**

| Samples | Tolerance factor(t') | Crystallite Size (D) in nm | Strain(η) |
|---|---|---|---|
| BFO-BST | 0.935 | 114.62 | 0.00215 |
| Nd1(x=0) | 0.929 | 71.28 | 0.00064 |
| Nd2(x=0.25) | 0.93 | 105.9 | 0.000133 |
| Nd3(x=0.5) | 0.928 | 104.12 | 0.000134 |
| Nd4(x=0.75) | 0.933 | 94.7 | 0.000199 |

The variables rA, rB, and rO represent the ionic radii of the A cation, B cation, and oxygen anion, respectively. The unit of measurement for these radii is angstroms (Å). In this example, we calculate the t-value by utilizing the ionic radius obtained from references. Specifically, we use the ionic radii of the A-site cations: rBi3+=1.40Å, rNd3+=0.995Å, rBa3+=1.61Å, r 3+=1.44Å; the B-site cations: r 3+=0.645Å, r 4+=1.44Å; and the X-site anion: r 2-=1.40Å. The derived t-values are then presented in Table 2. Since the values are more than 1, it may be concluded that all the compounds exhibit deviation from the ideal cubic structure.

**Micro-structural and Elemental analysis**

The Scanning Electron Microscope (SEM) was used to take images of the microstructural and surface morphological features of the sintered pellets. The SEM apparatus is fitted with an "EDAX (Energy Dispersive X-ray)" spectrometer to conduct elemental and compositional analysis of the samples. "The scanning electron microscope (SEM)" image of the sintered pellet made from BFO-BST is shown in Figure 1, while the images of the Series-II samples can be seen in Figure 2.

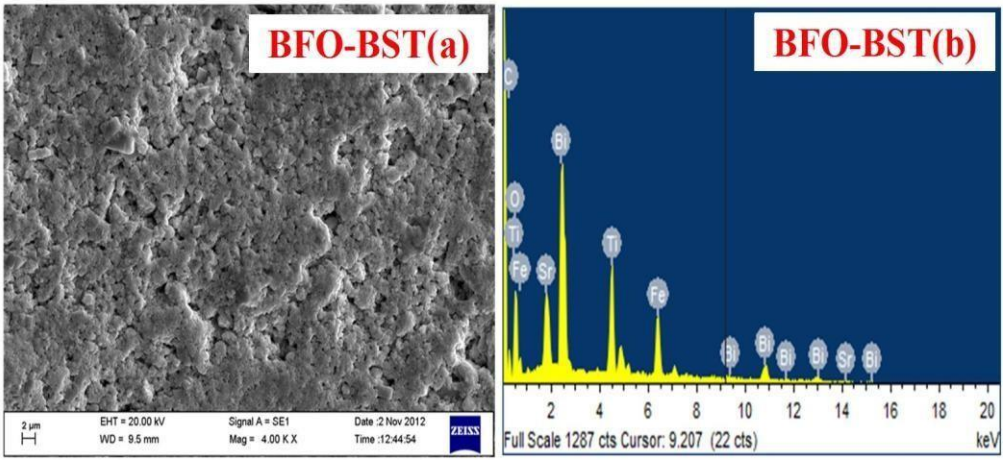


**Figure: 1 (a) SEM micrograph & (b) EDAX mapping of BFO-BST**[BiFeO3] 0.5 [(BaSr)0.5TiO3] 0.5

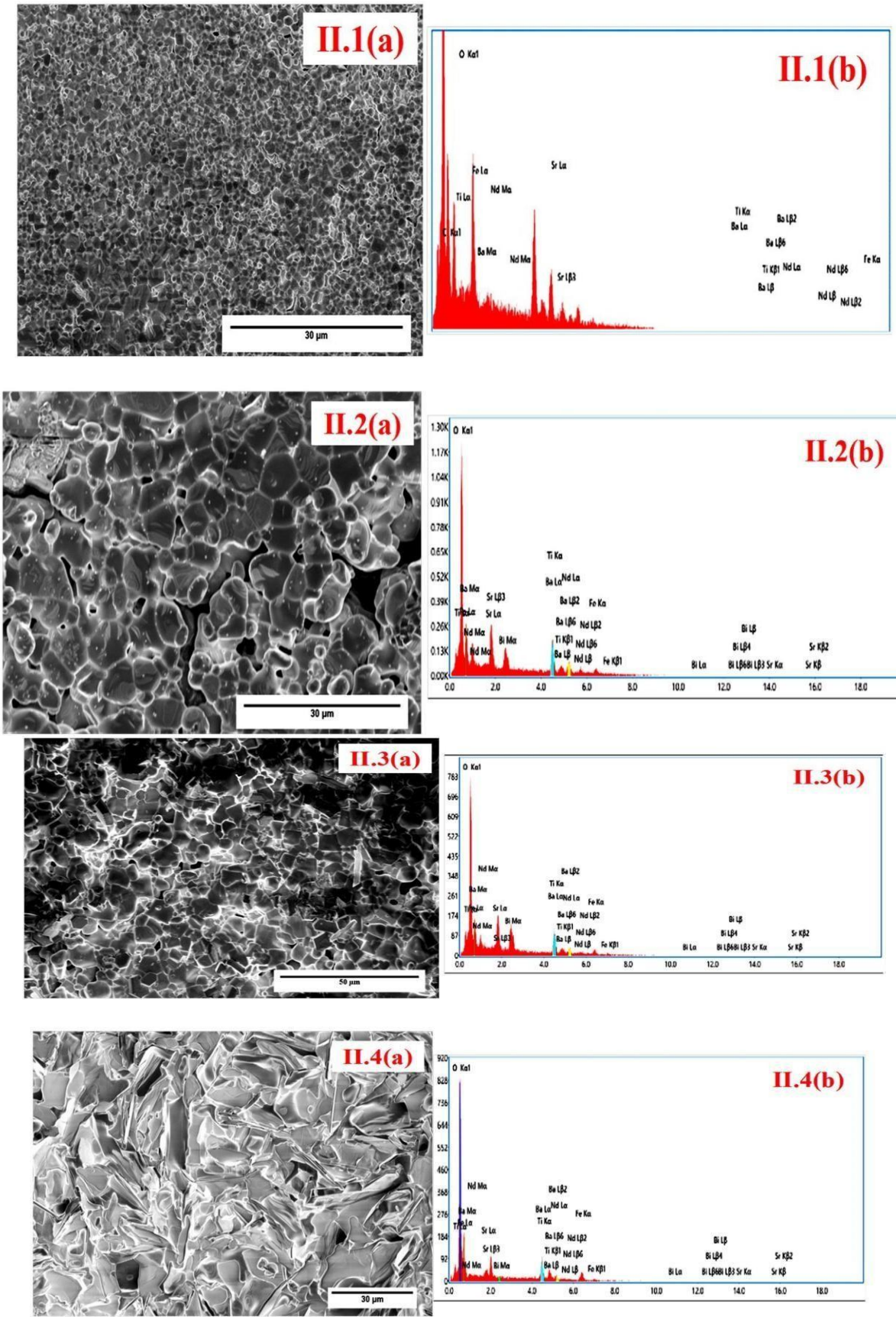


**Figure: 2. (a) SEM micrographs & (b)EDAX mappings of [BixNd(1-x) (BaSr)0.5]0.5[FeTi]0.5O3 (II.1).x=0, (II.2).x=0.25, (II.3).x=0.5 and (II.4).x=0.75.**

The micrograph obtained for BFO-BST exhibits agglomeration. The image displays distinct grain boundaries and voids, which serve as pathways for charge carriers to generate leakage. The system's lossy nature may be observed by the dielectric and polarization analysis, mostly caused by the impurity phase identified in the XRD diffraction pattern. The grain size of this chemical, determined using the intercept approach, is measured to be 1.435 micrometers. The micrographs depict the surface of [BixNd(1-x)(BaSr)0.5]0.5[FeTi]0.5O3 samples, where 0<x
The intercept technique was used to calculate the grain sizes for Nd1, Nd2, Nd3, and Nd4, which were found to be 1.38μm, 2.1μm, 1.84μm, and 1.52μm, respectively.

**Conclusion**

The SEM micrographs of our samples reveal polycrystalline microstructures in both the doped and host compounds. These microstructures exhibit well-defined grains and grain boundaries. However, the micrograph of the host compound reveals an agglomerated picture. When the concentration of x is changed from 0 to 0.75 in the doped samples, the presence of both Bi and rare earth (RE) ions in all three series of samples decreases the porosity in the systems. The decreased porosity suggests a decrease in the number of oxygen vacancies and an enhancement in the dielectric and multiferroic characteristics of the materials. The EDAX spectra of all samples indicate the presence of pure phases, as no traces of foreign elements were detected in any of the cases.

**References**


1. Wang N, Luo X, Han L, Zhang Z, Zhang R, Olin H, Yang Y. Structure, Performance, and Application of $BiFeO_3$ Nanomaterials. Nanomicro Lett. 2020 Mar 28;12(1):81. doi: 10.1007/s40820-020-00420-6. PMID: 34138095; PMCID: PMC7770668.
2. Verma, V. Structural, electrical and magnetic properties of rare-earth and transition element co-doped bismuth ferrites. *J. Alloys Compd.* **2015**, *641*, 205–209.
3. Tao, H.; Lv, J.; Zhang, R.; Xiang, R.; Wu, J. Lead-free rare earth-modified $BiFeO_3$ ceramics: Phase structure and electrical properties. *Mater. Des.* **2017**, *120*, 83–89.
4. Lam, S.; Jaffari, Z.H.; Sin, J. Hydrothermal synthesis of coral-like palladium-doped $BiFeO_3$ nanocomposites with enhanced photocatalytic and magnetic properties. *Mater. Lett.* **2018**, *224*, 1–4.
5. Arnold, D.C. Composition-driven structural phase transitions in rare-earth-doped $BiFeO_3$ ceramics: A review. *IEEE Trans. Ultrason. Ferroelectr. Freq. Control* **2015**, *62*, 62–82.